

Radiative-Auger transitions in soft-x-ray plasma emission

R. C. Elton and L. J. Palumbo*

Naval Research Laboratory, Washington, D. C. 20375

(Received 19 November 1973)

A broad, prominent emission blend is observed between 15 and 22 Å from a plasma produced in a θ -pinch deuterium discharge seeded with neon. The occurrence of this feature is associated with radiative-Auger-transition channels in various intermediate ion species, following the creation of short-lived 1s-orbit vacancies by the dielectronic capture of free electrons. The calculated blended spectrum from several stages of ionization agrees with the measured contour. A similar feature is detected near 27 Å with oxygen seeding. The measured intensities and shapes indicate that $2^1S \rightarrow 1^1S$ two-photon spontaneous emission in heliumlike ions is negligible for existing plasma conditions.

I. INTRODUCTION

One of the most fruitful regions of the spectrum for observing higher-order atomic processes is adjacent to strong $K\alpha$ -type inner-shell resonance lines which usually occur at high photon energy, i.e., in a relatively uncluttered region where weak "satellite" features can be observed in detail. Evidences of multiple (e.g., double-electron, double-photon) processes as well as nearly forbidden transitions have been repeatedly observed in this region, all of which provide insight into the finer details of atomic structure. It is of interest to extend such studies to highly ionized atoms where relatively simple systems can be created from heavier elements with increased nuclear charge and nucleus-electron interactions. A high-temperature plasma provides a convenient laboratory source of such ions at a sufficient density to permit spectroscopically resolved observations and with energetic electrons to provide the required excitation.

The present investigation and analysis concerns spectral regions on the long-wavelength sides of the strong resonance lines of the heliumlike Ne^{8+} and O^{6+} ions, and in particular relatively intense and broad features rising above the background continuum in the 15–22-Å and 25–30-Å regions, respectively. (A similar feature has recently been observed near 45 Å in a plasma created in a Tokamak device and is attributed to carbon impurities.¹) These integrated features are far more intense than the normal electron-ion bremsstrahlung emission and are also too narrow and distinct to be associated with this process.² Also, an observed gradual decay of the emission with increasing wavelength is in the opposite sense to that expected from electron-ion radiative recombination. An identification with an ion-atom association reaction emission is ruled out by the MeV-range ion energies required. The general shapes

of these features and the coincidence with a plasma electron kinetic temperature sufficiently high to produce the observed resonance line radiation initially suggested³ an association with two-photon emission from the $2^1S \rightarrow 1^1S$ transition in the heliumlike ions; however, the detailed intensity measurements and analyses described in this paper indicate that the emission is far too intense for this process or, furthermore, to result from simple electron-collisional excitation in *any single* ion for normal plasma conditions. Also, the measured intensity contour decays too rapidly with increasing wavelength for two-photon emission.

The broad emission may, however, be associated⁴ with a blend from inner-shell electron transitions in several ionic species. Indeed, it has been possible to obtain excellent agreement between the measured contour and a model in which the responsible radiative transitions involve two electrons simultaneously; i.e., a (small) portion of the $2p \rightarrow 1s$ electron transition energy is utilized by another bound electron in either an ionization or excitation transition, with the remainder of the energy released in a single photon. Such processes are usually referred to collectively as a "radiative-Auger" effect, and the resulting satellites to normal $K\alpha$ x-ray lines have been observed in heavier atoms.^{5–10} Theoretical studies complementing these observations have also been published.^{5, 9, 11} Radiative-Auger effects have been explained both from (a) an analogy with "shaking" effects common to β -decay^{11–13} and inner-shell photoionization¹⁴ (where the central potential acting on an electron is suddenly altered, resulting in its excitation during the rearrangement which follows) and (b) according to configuration interactions between final single-hole and double-hole states. The latter approach has been invoked^{8, 9} to explain anomalies not amenable to the former sudden-approximation approach. In explaining the emission pro-

file observed here, we will rely¹⁵ for convenience on the extensive theoretical and experimental results available for the shake-off and shake-up effects,¹⁶ even though the results may also be understood by configuration interactions (see Sec. IV C). In radiative-Auger transitions, shaking effects occur following the filling of a 1s vacancy and are more closely analogous to positron decay of the nucleus, the small additional effect of which has been included in one calculation.¹⁷

In a plasma, a vacancy in the 1s orbit can be created either by direct collisional removal of an electron, or by the dielectronic capture into a metastable complex of a free electron with the simultaneous promotion of an inner-shell electron (inverse to autoionization). In a recent study¹⁸ using a similar plasma device, it is shown experimentally that the latter process dominates. Also, the value for the electron temperature that is derived here from analyzing the relative spontaneous line emission from 2*p* to 1s electron transitions in Ne⁷⁺ and Ne⁸⁺ ions, assuming dielectronic capture into Ne⁷⁺, is consistent both with the value obtained from a laser light scattering experiment and with the predictions of a numerical model for the plasma. This temperature also leads to a consistent value for the electron density from the absolute Ne⁸⁺ ion line emission. These consistencies further support the dielectronic-capture model.

The observed dominance of the broadband emission over line radiation is explained by the transient existence of an electron in a quasi-bound-state from which ionization is probable; this is similar to a resonant scattering process. The intensities for the two broad features observed remain unexplained, since probabilities for the radiative-Auger stabilization channel from a quasi-stationary-state are unknown, and also since it has not been possible to time and space resolve the feature in the present experiment, i.e., the duration and exact location of the intermediate ion species relative to the higher species producing the line radiation is not known.

In Sec. II which follows, the experimental appa-

ratus and procedures are described, including those for the important intensity calibration. Only the (more accurate) relative intensity calibration over the wavelength region of interest is necessary for the analysis; however an extraction and use of the absolute intensity of the line emission from the Ne⁸⁺ ion adds assurance that this emission originates from a volume of "normal" plasma conditions. Following a presentation of the experimental observations in Sec. III, an interpretation of the observed spectral contour is given in Sec. IV according to the model described above for a blend of radiative-Auger emissions from several ionization stages. The paper concludes with a discussion in Sec. V of the importance of radiative-Auger transitions in the interpretation of soft-x-ray emission and radiative energy losses from high-temperature plasmas.

II. DESCRIPTION OF EXPERIMENT

A. θ -pinch device

The emission reported here was obtained from a plasma generated in a 50-kJ θ -pinch device.^{19,20} The plasma was formed within a single-turn coil of length 80 cm and was compressed radially from an initial diameter of 10 cm to a final diameter of ~ 2 cm and axially to a length of ~ 50 cm. The electrical characteristics are given in Table I. The sequence of operation began with two preionizer ring discharges, one beyond each end of the coil. A slowly rising antiparallel (to the main field) bias magnetic field was also introduced at this time by a current flowing through the main compression coil. This was followed after 10 μ sec by a low-energy preheating discharge through the compression coil. The main discharge began 25 μ sec after the initiation of the preionizer. The quartz chamber used was filled initially with deuterium (which was purified by passing through a heated palladium thimble) to a pressure of 15 mTorr, and heavier gases were added as desired. Since it was necessary to repeat the discharge cycle many times to obtain a spectrum (see Sec. III), an automatic gas-mixing and circuit-recycling

TABLE I. θ -pinch parameters.

	Main	Bias	Preheater	Preionizer
Total capacitance (μ F)	255	900	1.7	0.126
Charging potential (kV)	19.5	5.0	17.5	17.5
Energy (kJ)	48.5	11.3	0.26	0.019
Ring period (μ sec)	17	100	1.8	1.5
Inductance (nH)	29	280	50	450
Max. current (MA)	1.8	0.28	0.10	0.009
Max. field (kG)	29	-4.4	1.5	...
Firing time delay (μ sec)	25	0	10	0

system was devised²⁰ to maintain the maximum possible reproducibility in plasma conditions from one discharge to the next. The reproducibility was monitored through the discharge current as well as the time-resolved visible line radiation both from the atomic deuterium in the early stages of the discharge and from ionized impurity elements at later times. Streak photographs were taken in visible light through radial slots in the coil. Time-resolved (framing) visible-light photographs of the entire plasma were obtained through a perforated coil, particularly to determine the plasma dimensions. No axial plasma segmenting²¹ was observed at the low fill pressure and short plasma length present.

B. Grazing-incidence spectrograph

To obtain maximum emission and spectral resolution, the plasma was viewed axially with a 2.2-m grazing-incidence vacuum spectrograph. Although the instrument was equipped for photoelectric measurements, the intensity was too low for single-shot measurements, and multishot time-integrated photographic (plate) recording was used. A special gold-coated 600-grooves/mm grating²² with a blaze angle of 1.5° was used at an incidence angle of 87.5° from the normal. Kodak short wavelength radiation (SWR) plates were used in recording the data. A slit width as great as $24 \mu\text{m}$ was necessary to obtain sufficient photon flux for a reasonable number of discharges.

Baffles were placed before the entrance slit of the spectrograph to assure that only radiation from the plasma was recorded; i.e., impurity radiation near the walls could not enter the spectrograph. The interior of the spectrograph was also carefully baffled to prevent scattered radiation from reaching the plate. A soot-blackened central-image trap was necessary to prevent plate-fogging from this radiation. No visible-light plate-fogging was detected through a 6-mm-thick quartz window, following these procedures.

Because of the construction of the spectrograph and the low grazing angle used, the short wavelengths of interest fell close to the end of the photographic plate. For this reason, and to better approach the optimum blaze wavelength ($\sim 60 \text{ \AA}$ first order), the neon spectrum was observed in second order with the overlapping first order efficiently reduced by thin filters of both VYNS-3 (copolymer consisting of nine molecules vinyl chloride per vinyl acetate molecules; specific gravity²³ = 1.39) and aluminum. Large areas of VYNS-3 were readily prepared²⁴ in $0.3\text{--}1.0 \mu\text{m}$ layers for high transmission, but were only useful for wavelengths shorter than the L edge of chlo-

rine, measured here to be at 61.5 \AA . The aluminum filter is essentially opaque from 30 to 172 \AA . A large reduction in intensity from strong first-order carbon-ion lines in the vicinity was an indication of the efficiency of these filters.

C. Spectrograph intensity calibration

For analysis of the second-order neon spectrum, both relative and absolute instrumental sensitivities were determined for the grazing-incidence spectrograph over the true wavelength range of $12\text{--}23 \text{ \AA}$ and for the photographic density range of the data. This calibration was performed (see Fig. 1) using a Henke-type²⁵ high-current dc x-ray source which emitted strong-line radiation from anode elements of Zn, Cu, F, and O. A flow proportional counter was used to measure the photon flux entering the spectrograph slit,²⁶ and the calibration was performed through filters identical to those used in obtaining the data from the plasma. The counter was operated at atmospheric pressure in $P\text{-}10$ gas (90% argon, 10% methane) and at a potential of $1500\text{--}2000 \text{ V}$ with an energy resolution close to the theoretical limit.²⁷ Because the resolution is limited for such a counter, the spectra from the x-ray tube were also measured with a Bragg rotating-crystal spectrometer to identify possible blended impurity lines. Details of the calibration techniques involved are available elsewhere.²⁰

The resulting measured instrumental sensitivity in units of exposure on the photographic plate per photon cm^{-2} at the entrance slit is shown as a function of wavelength in Fig. 2 for second order. In order to simulate the observed spectral feature with computations, the spectrograph sensitivity data of Fig. 2 had to be rendered into a computer-compatible form. This was done by approximating the sensitivity with a second-order polynomial whose coefficients were derived by a least-squares fit to the data points in Fig. 2 and to an additional point (needed to straddle the spec-

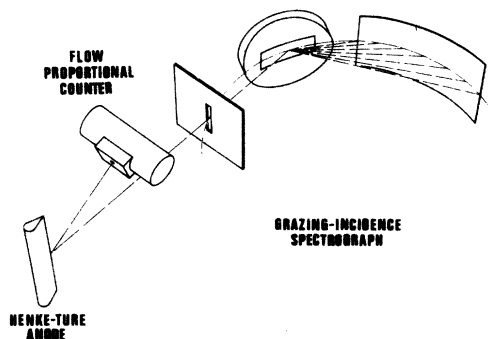


FIG. 1. Schematic of method for intensity calibration of grazing-incidence spectrograph.

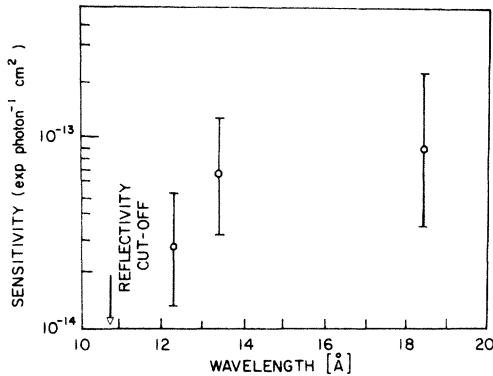


FIG. 2. Second-order absolute sensitivity vs true wavelength for grazing-incidence spectrograph in exposure units (exp, consistent with Fig. 3) per photon cm^{-2} at the entrance slit. A data point at 25 \AA was deduced as discussed in text. Kodak type SWR emulsion used.

tral range of the observations) at 25 \AA where the sensitivity was estimated to be 1.5×10^{-13} exposure units per photon cm^{-2} . The choice of this point ensured that the instrument sensitivity increased monotonically with wavelength with a slope approximately equal to that expected from both rough-grating reflectivity calculations and from calibrations on similar instruments.^{26,28} The selection of the above value for sensitivity at 25 \AA is further supported by a calibration measurement on the present spectrograph which provided a lower limit for sensitivity at 23.7 \AA (oxygen $K\alpha$).

The density-versus-exposure data necessary to complete this calibration are shown in Fig. 3 for both Kodak types SWR and 101 emulsions. (The latter showed excessive surface irregularities and could not be used for data collection on

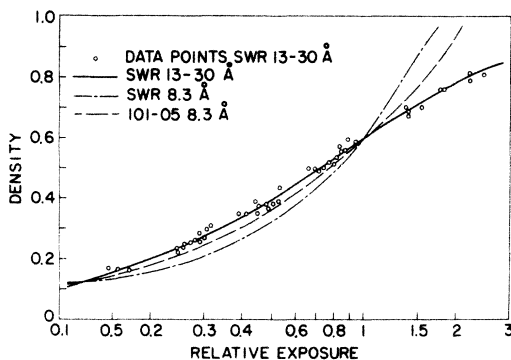


FIG. 3. Plate density vs exposure for Kodak types 101 and SWR emulsions for wavelengths shown. Exposure scale (same for 8.3 and 13–30 \AA SWR data) is normalized such that an exposure of unity produces a density of 0.6 and is consistent with Fig. 2. Absolute exposure for type 101 emulsion $\approx 1/6$ that of type SWR at same density.

the θ -pinch; it proved useful in the relative calibration, however.) The over-all accuracy of the relative calibration was judged to be $\pm 15\%$. The spectroscopic data for the double-electron transitions are reduced below, using only this relative calibration. The absolute calibration, which is used below to deduce a consistent value for the plasma electron density from the Ne^{8+} ion line radiation, is considered to be accurate to within a factor of 3. Failure of the reciprocity law between the dc calibration and the 1–5- μsec plasma exposures is not expected to affect appreciably the calibration, since grain activation is expected to occur from single-photon exposure in this energy range.²⁹

III. OBSERVATIONS

The spectra were photographed in second order through an $\sim 4000\text{-\AA}$ -thick VYNS-3 filter by superimposing sequences of first 30 and then 50 discharges at plate positions partially shifted parallel to the spectral lines, so as to provide a central overlap exposure from 80 discharges. This technique provided density-versus-exposure information directly from the data plate over the wavelength range covered, by using lines of various exposure. Densitometer tracings of the spectra obtained for 80 discharges with 12% neon and with 6% (molecular) oxygen added to a 15-mTorr deuterium fill gas are shown in Figs. 4 and 5. All

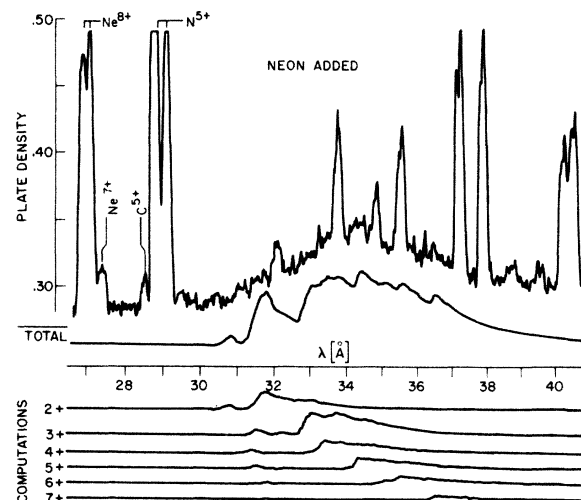


FIG. 4. Comparison between a densitometer tracing of the time-integrated second-order neon prominence and a computed blend of radiative-Auger emission (converted to photographic density using Figs. 2 and 3 for SWR emulsion). Relative contributions from each ionic species are also shown in density units. A 5% contribution from radiative-excitation-type transitions is included here.

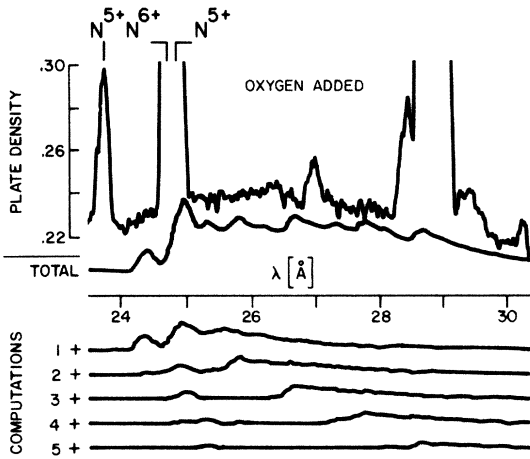


FIG. 5. Comparison between a densitometer tracing of the time-integrated first-order oxygen prominence and a computed blend of radiative-Auger emission (converted to photographic density using Figs. 2 and 3 for SWR emulsion). Relative contributions from each ionic species are also shown in density units. A 15% contribution from radiative-excitation-type transitions is included here.

of the major lines in these spectra have been identified^{3, 30, 31} as originating in highly stripped ions of carbon, nitrogen, oxygen, and neon.

The broad feature between 30 and 44 Å (second order) shown in Fig. 4 appeared only in the presence of strong resonance-line radiation from the Ne⁸⁺ ion, and is associated with a sufficiently high electron kinetic temperature to excite the K α -type lines in this and lower ionic species of neon. The direct association with neon ions was confirmed by repeating the measurements with 6% (molecular) oxygen, under which conditions the same feature did not appear, and an

additional feature appeared between 25 and 30 Å (first order) as shown in Fig. 5; the latter is associated below with similar radiative-Auger transitions in oxygen ions. As further verification, the neon spectrum was repeated (with 160 discharges) using an ~7500-Å-thick aluminum filter, which has no absorption edges in the vicinity, and the third and fourth orders of the feature were recorded as well.

The measured absolute plasma emissions are listed in Table II for the neon feature as well as for nearby relevant lines. The absolute intensities are given mostly for completeness, since it is the relative intensity (~15% precision) which is of importance in explaining below the source of the prominent broadband emission and in deducing an electron temperature for the plasma. The absolute intensity ($\times 3$ accuracy) of the 2^3P-1^1S line of the Ne⁸⁺ ion is only used in deducing a value for the electron density.

IV. INTERPRETATION

In order to properly identify the origin of the observed features, a model capable of simulating the observations as closely as possible must be developed. Such a model should first be capable of predicting the over-all contour of the feature as well as any reproducible discrete structure detected. If possible, the observed intensity should also be predictable. Finally, any further predictions of the particular model chosen should be consistent with observations.

A. Contour

Concerning the shape and structure of the features, the instrumental calibration allows us to conclude that the true emission decays with in-

TABLE II. Measured neon line and continuum emission per discharge from the plasma according to the data shown in Fig. 4. The relative precision is expected to be $\pm 15\%$ and the absolute precision $\times 3$. The emission is over 4π steradians.

Species	Transition	Wavelength (Å)	Emission (10^{16} photons)	Power density ^a (10^4 W/cm ³)
Ne ⁸⁺	$1s2p^3P \rightarrow 1s^2^1S$	13.55 ^b	6.4	1.2
Ne ⁷⁺	$1s(2^1S)2s2p(^4P)^2P \rightarrow 1s^22s^2S$	13.65 ^c	1.28	0.22
	$1s2p^2^2D \rightarrow 1s^22p^2P$	13.71 ^c		
Ne ²⁺ -Ne ⁷⁺	$1s2s^j2p^k \rightarrow \begin{cases} 1s^22s^{j-1}2p^{k-1}ns \\ 1s^22s^j2p^{k-2}np \\ (n=3, \infty) \end{cases}$	15-22	160	Note d

^a Volume is 160 cm³; exposure time is 5 μ sec.

^b See Ref. 31.

^c See Ref. 39.

^d Volume and exposure time are variable for blended species.

creasing wavelength much more rapidly than can be explained by the originally proposed³ model of $1s2s^1S \rightarrow 1s^2^1S$ two-photon emission,³² although the short-wavelength portion remains consistent with a reduced resonance-photon energy. The shape is remarkably similar to that familiar in $K\alpha$ -satellite x-ray spectra and associated with radiative-Auger transitions, where radiation from a $2p \rightarrow 1s$ transition is accompanied by the release of a valence electron. It is this two-step process, i.e., the filling of a $1s$ -orbit vacancy by a $2p$ electron and the promotion of another electron, that has been successfully applied here in explaining the observed detailed contour. The complete model must include creation of the initial $1s$ -orbit vacancy and this is developed as needed, first to estimate the relative emission for each ion and finally to satisfy the over-all consistency requirements for the model.

The dominant mode of that radiative-Auger decay process which results in ionization may be described for low- Z ions by

$$1s2s^j2p^k \rightarrow \left\{ \begin{array}{l} 1s^22s^j2p^{k-2} \\ 1s^22s^{j-1}2p^{k-1} \end{array} \right\} + h\nu + e, \quad (1)$$

where $0 \leq j \leq 2$, $1 \leq k \leq 6$, $j+k \geq 2$. The main ($2p \rightarrow 1s$) transition is electric dipole,⁹ with the energy shared by the photon $h\nu$ and the released electron. Monopole decay⁵ ($2s \rightarrow 1s$) is also possible as a double-dipole transition, but is neglected here since the yield is expected to be much lower than for dipole decay.³³ Promotion of an alternate $2s$ or $2p$ electron is assumed to occur as a *result* of the filling of the $1s$ -orbit vacancy and is therefore considered to be governed by monopole selection rules,^{9,34} which considerably reduces the number of possible transitions.³⁵ A continuous spectrum of photons results corresponding to the range of kinetic energies for the ejected electron, the distribution of which is given by calculations for β decay and from experiments on photoionization. Promotion of the alternate electron to a higher bound state is also possible, with a probability decreasing rapidly¹² with increasing principal quantum number. Such excitation to $n=3$ orbits was included in the numerical modeling in sufficient amounts to fit the measured results.

The total radiative-Auger emission rate per cm^3 is given by $N_{i0}N_ePY_{ra}$, where N_{i0} is the density of ions in the initial state (no $1s$ vacancies), N_e is the electron density, P is the total rate coefficient for $1s$ -vacancy production, and Y_{ra} is the branching ratio for the radiative-Auger process. In order to evaluate this for any particular ion,

it is necessary to know the relative population rate N_eP for the various possible excited terms formed from each significantly populated initial term of density N_{i0} . The most likely mechanism for $1s$ -orbit vacancy production in θ -pinch plasmas has been found¹⁸ to be by electron-ion dielectronic capture, whereby a $1s$ electron is promoted to a higher bound orbit during the collision of an ion with a free electron which has subthreshold kinetic energy for direct excitation or ionization. The rate coefficient P for this process and for a particular ionic configuration is determined by detailed balancing³⁶ to be proportional to $(\omega_f/\omega_i)A_aS$, where ω_i and ω_f are statistical weights for the initial and final terms, respectively, A_a is the autoionization rate for the final term, and $S(T_e)$ is a Saha function dependent on the electron temperature T_e .

The total spectral profile for a particular excited term formed from a particular initial-ion term thus scales as $(\omega_f/\omega_i)N_{i0}A_a$, assuming constant values for N_e , T_e , and Y_{ra} , and this relation is used in computing the expected shape for each ionic species. (The justification for this assumption concerning Y_{ra} is that all double-electron transitions involved, i.e., radiative and non-radiative Auger, scale the same with ionization, and that the spontaneous radiative-decay contribution is negligible compared to the total decay rate for low- Z ions.^{37,38}) Mean values for the autoionization rates A_a for those terms within a (final) configuration which are allowed to autoionize are obtainable from recently calculated averaged (over *all* terms and weighted according to statistical weights) Auger rates for both neon³⁷ and oxygen³⁸ ions. These are obtained for both $2s2p$ and $2p2p$ active-electron combinations by multiplying the calculated Auger rates by the total statistical weight ω_T for all terms in a given configuration and dividing by the total statistical weight for those terms permitted to autoionize. Since no more detailed information is known on term dependence, such mean values must suffice. The results used for configurations important in the present analysis (many are not required due to insignificant initial term populations as discussed below) are collected in Table III. For the Ne^{7+} and O^{5+} lithiumlike ions it has been possible to obtain separate rates for the $1s(^2S)2s2p(^1P)$ and $1s(^2S)2s2p(^3P)$ configurations by equating the calculated Auger rate to a statistically weighted average of the autoionization rates for these two configurations and requiring approximately a 4:1 ratio, respectively, for the autoionization rates, according to recent calculations.^{39,40} The branching ratio Y_{ra} was divided between $2s2p$ and $2p2p$ active-electron combinations for all stages of

TABLE III. Autoionization rates $A_a \times 10^4 / \text{atu}$ for configurations of total statistical weight ω_T and terms shown in neon and oxygen ions populated by dielectric capture and allowed to decay by radiative-Auger transitions ($1 \text{ atu} = 2.42 \times 10^{-17} \text{ sec}$).

Configuration	ω_T	2s-2s		2s-2p		2p-2p				
		Terms	$A_a(\text{Ne})$	$A_a(\text{O})$	Terms	$A_a(\text{Ne})$	$A_a(\text{O})$	Terms	$A_a(\text{Ne})$	$A_a(\text{O})$
$1s2s^22p^6$	2							2S	55.3	
$1s2s^22p^5$	12							$^1P, ^3P$	45.4	
$1s2s^22p^4$	30							$^2S, ^2P, ^2D, ^4P$	33.1	22.5
$1s2s^22p^3$	40				$^3S, ^3P, ^3D, ^5S$	24.6	18.9	$^1P, ^1D, ^3P, ^3D$	24.7	18.0
$1s2s2p^4$	60							$^2P, ^3P, ^4P, ^3D, ^5P$	47.9	35.1
$1s2s^22p^2$	30				$^2S, ^2P, ^2D, ^4P$	15.2	12.2	$^3S, ^2D$	19.2	15.0
$1s2s2p^3$	80							$^1P, ^2P, ^3P, ^2D, ^1D, ^2D, ^3D, ^4P, ^4D$	28.1	21.8
$1s2s^22p$	12	$^1P, ^3P$	15.4	13.2	$^1P, ^3P$	8.61	7.25			
$1s2s2p^2$	60				$^1S, ^1P, ^1D, ^3S, ^2P, ^3P, ^4P, ^3D$	11.3	9.47	$^1S, ^1D, ^3S, ^3D$	21.7	17.7
$1s2p^3$	40							$^1P, ^1D, ^3P, ^3D$	31.6	21.8
$1s(^2S)2s2p(^1P)$	6				2P	10.75	9.36			
$1s(^2S)2s2p(^3P)$	18				2P	2.69	2.34			
$1s2p^2$	30							$^2S, ^2D$	24.2	20.6

ionization according to an expected 1:4 ratio, obtained from available data for a change in screening due to photoionization from the 1s orbit.⁴¹ (Such data seem more appropriate than those from β decay¹⁷ for the present application.) The required statistical weights ω_f for the final terms correspond to those terms listed in Table III; those for the initial terms ω_i correspond to the relevant initial terms as discussed below. For the portion resulting in ionization, the detailed wavelength distribution of the photon emission was determined using Eq. (24) of Ref. 12 for the distribution of free-electron energy following shake-off. Finally, the branching ratios between transitions ending in ionization or excitation for oxygen and neon were introduced as adjustable parameters for best fit to the data for each element.

In computing the contribution from each excited ionic term, the energies for the excited configurations were obtained from calculations⁴² and those for the final configurations from the combined binding energies of the electrons determined from tabulated ionization potentials⁴³ and wavelengths³¹ and from calculated energy levels.⁴⁴ From 1 to 13 excited ionic terms are populated by dielectronic capture from signifi-

cantly populated ground-state terms and are allowed to decay by radiative-Auger ionization into from one to nine low-lying terms (filled 1s orbit) of the next higher stage of ionization; from 6 to 58 of such transitions have a nonzero probability depending on the species. For radiative-Auger transitions involving excitation, an average (per ionization stage) of 75 transitions from terms with a 1s-orbit vacancy into terms with configurations of the form $1s^22s^x2p^y3l$ had to be considered.

The relative initial-ion term populations N_{i0} were included as follows for neon ions (the results were also applied to the isoelectronic oxygen ions). The analysis began with the Ne^{8+} ion, since the density of Ne^{9+} ions is insignificant as evidenced by the absence of the Ly- α line. In the formation of Ne^{7+} ions from Ne^{8+} , only the $1s^2\ ^1S$ initial ground term is involved; the $1s2s\ ^3S$ "metastable" term is not significantly populated since it is not formed by autoionization of Ne^{7+} and since the rates for electron-collisional depopulation both to the $1s2p\ ^3P$ term (for which the $J=1$ level decays rapidly⁴⁵ to the ground term) and to the continuum through ionization^{46, 47} greatly exceeds the population rate from the ground term.^{48, 49} (Metastable-state depopulation by Auger transitions is forbidden by energy con-

siderations for the singly excited initial states considered here.) For dielectronic capture onto Ne^{7+} ions to form Ne^{6+} , about equal population densities were assumed for the $1s^2 2s^2 S$ and $1s^2 2p^2 P$ initial terms, since $2s-2p$ electron-collisional excitation⁵⁰ is balanced by collisional deexcitation and radiative decay⁵¹ for the close spacing involved and for the electron density derived in Sec. IV D below. In forming Ne^{5+} excited ions, a population density for the low-lying $1s^2 2s2p^3 P$ "metastable" term in the Ne^{6+} ion was assumed to be equal to about one-half of that for the $1s^2 2s^2 {}^1S$ ground term from a measurement on a similar θ -pinch device.⁴⁷ This ratio is much less than the thermal equilibrium value of 9:1 and depends on a balance between electron-collisional excitation from the ground term⁵² and deexcitation both by the inverse collisional transition as well as by electron spin-exchange transitions (with a rate coefficient of $\sim 10^{-10} \text{ cm}^3 \text{ sec}^{-1}$ expected⁵³) to the $n=2$ singlet terms. This ratio will be density independent, since only electron-collisional rates are involved.

For lower ionic species, data do not exist such as are available for the higher species, and rough estimates are necessary. In forming Ne^{4+} , the population of the $1s^2 2s2p^2 {}^4P$ metastable term in the Ne^{5+} ion must be accounted for, as well as the $1s^2 2s^2 2p^2 P$ ground term. The excitation rate of the $2 {}^4P$ term from the ground term⁵² was taken as the dipole rate given by the Bethe-Born approximation^{46, 54} divided by 15 (from the available Ne^{6+} data⁵³); the deexcitation rate was determined by detailed balancing, and the $2 {}^4P-2 {}^2P$ rate coefficient was taken as $10^{-10} \text{ cm}^3 \text{ sec}^{-1}$ again by analogy to the Ne^{6+} data. The resulting population density ratio $N(2 {}^4P)/N(2 {}^2P)$ is approximately one-half, which is less than the thermal equilibrium value of 2 (as was the case for the Ne^{6+} ion). Data also do not exist for forming excited Ne^{3+} ions. However, in the initial Ne^{4+} ion, the $1s^2 2s^2 2p^2 {}^1S$ and 1D terms are sufficiently close to the ground term to be in thermal equilibrium. Because of a low statistical weight, the population of the 1S term is neglected and that of the 1D term taken to be $\frac{5}{9}$ that of the 3P ground term, according to the statistical weight ratio. An estimate of the population of the $1s^2 2s2p^3 {}^5S$ metastable term was made in a similar fashion to that for the $2 {}^4P$ term in Ne^{5+} above, using a $2 {}^5S-2 {}^3S$ exchange-rate coefficient of $10^{-10} \text{ cm}^3 \text{ sec}^{-1}$ again^{48, 49, 55, 56} and accounting for ionization from the excited $n=2$ triplet levels.^{46, 57} This population was found to be negligibly small. For Ne^{3+} and Ne^{2+} ions (Ne^{2+} included in the analysis but of negligible importance, as was Ne^{1+} forming neutral neon), which form Ne^{2+} and Ne^{1+} , respec-

tively, the $n=2$ metastable terms are sufficiently close to the ground term and removed from higher terms to assume an equilibrium statistical distribution to exist according to electron-collisional spin-exchange excitation and deexcitation. While these estimates for metastable population densities are approximate, the only effect of their inclusion is in the finer structure of the gross contribution for each species as shown in Figs. 4 and 5; i.e., they are included mainly for completeness.

The numerical results of this modeling for several neon ions are included in Fig. 4, along with a densitometer tracing of the total feature. Computed and measured contours may be compared directly, since the former have been corrected for instrument efficiency and converted to plate density. The finite spectrograph resolving power was included by convolution. Shown in Fig. 4 is a computed blend as well as the individual contributions from each ionic species, with the emission weighted empirically according to factors of 8, 10, 6, 5, 4, and 2 for emissions from Ne^{2+} through Ne^{7+} ions, respectively. A 5% contribution from transitions ending in excitation is included here for a best fit at the shorter wavelengths.

The blended-contour comparison for oxygen ions is shown in Fig. 5, where empirical weighting factors of 10, 6, 5, 4, and 2 have been used for O^{2+} through O^{6+} ions, respectively. A 15% contribution for the excitation mode was included for best fit. In the case of oxygen, the hydrogenic ion O^{7+} is generated in the plasma as evidenced by the presence of the Ly- α line; however the analysis was not extended to include contributions arising from the presence of this ion since the relative contribution from the higher species has already been indicated to be small; in any case, no significant emission is found in the region of the predicted O^{6+} edge at 30.3 \AA . Since the oxygen broadband emission occurs in first order and the present instrumental calibration is limited to second order, a first-order calibration²⁸ completed on a similar instrument was adequate for computing the relative oxygen emission for the rather narrow wavelength band ($\sim 5 \text{ \AA}$) involved.

B. Intensity

It is clear from the results of the instrumental calibration that the broadband emission relative to that from the nearby heliumlike resonance lines is far too intense to be explained as a satellite feature evolving from this ion alone. (The fact that the features are observed only under conditions where the heliumlike resonance lines

are also emitted is most likely due to the requirement of high-energy electrons for $1s$ -electron promotion and not to a more direct correlation.) The association above with a blend of contributions from various ionic species aids in explaining the large intensities observed, although other indicators (such as line radiation) for these species are absent in this spectral region. Recalling that the present results were necessarily limited (by the low sensitivity of the detection apparatus) to time- and space-integrated measurements, it is clear that no further understanding can be gained concerning the emission level; i.e., the broadband emission may be occurring in different regions and for different time intervals than for any particular nearby spectral line to which it might be compared. Likewise, no definite conclusions can be drawn concerning the intensity ratio between the neon and oxygen features.

C. Self-consistency

For any model, observations should be consistent with all predictions. In radiative-Auger decay (ignoring the $1s$ -vacancy production phase), $K\alpha$ -type inner-shell lines should be present, as well as satellite lines due to the promotion of bound electrons to higher discrete levels. From shake-up theory for low-lying orbits in ionized species, the latter blended lines are expected to contribute at the short-wavelength end of the feature ($\sim 16 \text{ \AA}$ in neon) and could be expected to represent up to 23% of the total radiative-Auger emission.¹² This effect was included in the model as described above, but the resulting emission was found to be weak in the experiment (5% for neon, 15% for oxygen from best-fit analyses). Also, except for the lithiumlike ionic species, no $K\alpha$ -type inner-shell radiation was observed.

In order to explain the apparent absence of strong inner-shell line radiation in the presence of prominent radiative-Auger emission, it is necessary to adopt a mechanism for $1s$ -orbit vacancy production which can produce quasi-stationary "would-be-bound states"^{58, 59} with the captured electron in broad, quasidecrete levels from which it preferentially leaves through autoionization (Auger) or radiative-Auger transitions. In the dielectronic capture excitation model adopted above, such a metastable complex is formed and may be considered as a subthreshold resonance in the scattering of free electrons from ions.⁵⁸ Following "capture," stabilization may occur through various channels such as (a) radiative decay (rearrangement collision with radiative recombination), (b) autoionization (elastic scattering collision), or (c) radiative-Auger (re-

arrangement with bremsstrahlung-type emission). [Radiative decay with alternate-electron *excitation* may be considered a subchannel of (a) in this context, with two photons emitted as line radiation in the final stabilization.] Thus the observed prominent emission might be considered as a resonance in the normal electron-ion bremsstrahlung emission, with the intensity described by interactions between discrete and continuum configurations. The observed preference for re-emission of the captured electron implies a short interaction time compared both to a bound electron orbit time and consequently also to the lifetime of the excited state. Whether the dominant continuum emission (over line emission) is associated with a broadened contributing free-electron energy distribution (associated with a short lifetime) or with a preference for $1s$ -electron excitation into a variable-energy virtual state^{59, 60} with an excited inner-shell electron below the $2p$ level is not resolved.

In the simplified contour model adopted above, radiative-Auger electron emission from a discrete bound state (shake-off/shake-up model) was assumed for convenience, rather than a quasi-continuum distribution of energies. The effect of this assumption on the numerical results has been discrete steps (except for an included instrumental smearing effect) for each species indicated in Figs. 4 and 5. This has aided in identifying the proper relative contribution to be included for each ion. The added effect of further smoothing of the edges due to quasidecrete levels is evident in the experimental data.

D. Plasma conditions

A specific knowledge of plasma conditions was not essential in completing the above analysis. However, since the broad features were observed only when characteristic line radiation from the heliumlike species was present, it is of interest to ascertain that this line radiation corresponds to normal plasma conditions for a θ -pinch device, that the measured electron temperature is sufficiently high to assure abundant high-energy electrons for inner-shell excitation, and that the dielectronic-capture excitation model adopted, when used to deduce an electron temperature, gives a consistent value, i.e., that it is a valid model for inner-shell excitation in this plasma.

A value for the electron temperature T_e is obtained independently of any knowledge of the electron density from a comparison of the spontaneous emission $I(7+)$ from the $1s(2S) 2s2p(1P) 2P - 1s^2 2s^1 S$ inner-shell line of the Ne^{7+} ion at 13.65 \AA with the emission $I(8+)$ from the optically thin $1s2p^3 P$

$-1s^2\ ^1S$ intercombination line of Ne^{8+} at $13.55\ \text{\AA}$. It is assumed that the former line forms by dielectronic recombination and the latter line by electron collisional excitation from the ground level.^{46,54} The intensity ratio is given by^{18,39}

$$\frac{I(7+)}{I(2+)} = \frac{\sqrt{3}}{4} \frac{a_0 \omega_f A_{rd}}{\alpha c f \langle g \rangle} \left(\frac{E_i^* - E_i}{kT_e} \right) \exp\left(\frac{E_i^* - E_i}{kT_e} \right), \quad (2)$$

where $\langle g \rangle = 0.2$ is an effective Gaunt factor averaged over a Maxwellian velocity distribution, $\omega_f = 6$ for the $1s(2S)2s2p(1P)^2P$ term, A_{rd} is the radiative decay rate for the Ne^{7+} -ion line (numerically equal to $1.74 \times 10^{-4} \text{ au}^{-1}$ or $7.2 \times 10^{12} \text{ sec}^{-1}$), E_i and E_i^* are, respectively, the binding energies of the ground and excited states of the Ne^{8+} ion, E_f is the binding energy of the Ne^{7+} $1s(2S)2s2p(1P)^2P$ term, α is the fine-structure constant, and a_0 is the Bohr radius. The oscillator strength f is taken as 0.55 from that for $1^1S - 2^1P$ excitation,³⁹ since the rate for this transition is approximately equal (within 10%) to that for the total $1^1S - 2^3S + 2^3P$ excitation which leads to the intercombination line emission (assuming the depopulation rate of the $n=2$ triplet levels by spin-exchange collisions to be small compared to the radiative decay rate to the 1^1S ground level).^{48, 49, 61} Equation (2) yields an electron kinetic temperature of $kT_e = 150 \text{ eV}$ for a measured intensity ratio of 0.1 (Table II), recalling that $I(7+)$ here is approximately one-half of the Ne^{7+} satellite-line blend.¹⁸

A value for the electron density in the plasma is determined from the measured absolute intensity from the Ne^{8+} intercombination line (see Table II), which is optically thin because of the low oscillator strength. The total intensity of this line is again determined by the electron-collisional excitation rate into the upper $1s2p^3P$ term and is given by $N_e N_i X(i, i^*) V \Delta t$, where $X(i, i^*)$ is the excitation-rate coefficient,^{46, 54} V is the volume of the emitting plasma ($\approx 160 \text{ cm}^3$) and $\Delta t \approx 5 \mu\text{sec}$ is the time interval for the emission, determined both from a numerical model (see below) and from time-resolved soft-x-ray measurements near $15\ \text{\AA}$ through a thin ($3 \mu\text{m}$) nickel foil. Accounting for the eight electrons contributed from each neon atom as well as those from the deuterium atoms, an electron density of $N_e = 6 \times 10^{16} \text{ cm}^{-3}$ is deduced.

These measured values for electron temperature and density are in very close agreement with calculated values for this particular plasma (shown in Fig. 6) using a numerical model for θ -pinch plasmas⁶² which yields a peak electron kinetic temperature of $kT_e = 145 \text{ eV}$ and density of $N_e = 6.2 \times 10^{16} \text{ cm}^{-3}$, with a Ne^{8+} -ion existence interval of $\sim 5 \mu\text{sec}$. The electron temperature deduced is also in close agreement with that found from

90° laser light scattering.⁶³ The predicted ion temperature T_i rises slower than the electron temperature and approaches T_e (within 20%) at $7 \mu\text{sec}$.

From the results of the numerical simulation of plasma conditions shown in Fig. 6, it is seen that the electron temperature reaches 70% of its peak value at $1.2 \mu\text{sec}$ when the Ne^{3+} ion is present and the electron density has risen to greater than 10^{16} cm^{-3} , so that there is a sufficient density of high-energy electrons present to generate K -shell vacancies in this and higher stages of ionization. [The heliumlike ions (such as Ne^{8+}) are often the terminal point, since their ionization potential is always much greater than the lower stages.] Measurements of the contributions from each ion stage are not possible at the low signal levels available.

V. DISCUSSION

The shapes of the pronounced features observed in the soft-x-ray continuum plasma spectra are explained as blended emission from radiative-Auger transitions following the creation of $1s$ -orbit vacancies by inelastic electron-ion resonance collisions in various ionic species. Such

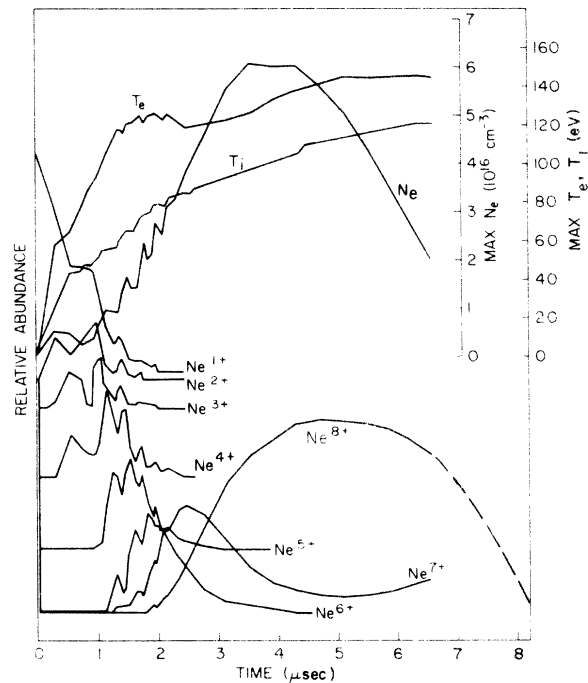


FIG. 6. Numerically predicted spatially-integrated population evolution for the neon ionization stages and the maximum (radially) electron density and electron and ion temperatures. Only sequential ionization and radiative recombination are included.

radiation represents a new energy-loss mechanism for the plasma, as the free electrons are captured and subsequently released with considerably reduced energy, with the excess energy converted to radiation. For example, in the present experiment the total emission from the feature associated with neon is measured (Table II) to exceed the expected total bremsstrahlung and recombination emission^{2, 46} for the plasma parameters and volume given in Sec. IV, although again the specific regions of radiation are not resolved. The importance of this emission to the energy balance in a specific plasma,^{46, 64} is not easy to predict at present, since the relevant process rates for contributing ions are not well known and the population densities of the various ionic species present are often not known as functions of time and space. Unfortunately, the present experiment cannot provide further information on the specific rates, since the emitting volume and duration for each species is not measurable. However, with what is presently known, it is reasonable to assume that the presence of solely hydrogenic and heliumlike species of light elements in high-temperature plasmas is not likely to result in significantly increased radiative losses due to radiative-Auger processes.

Radiative-Auger emission would seem to be most important both in a plasma (such as generated here) where the initial electron heating rate ex-

ceeds the impurity ionization rate so that several intermediate stages of ionization can contribute, and in hot quiescent plasmas in which cold impurity ions are likely to enter more rapidly than they are stripped of outer electrons. To better understand the significance of this process, it is clear that observations under more favorable conditions for detailed localized measurements (perhaps forthcoming¹) are required, as well as further theoretical studies on the radiative-Auger stabilization channel.

VI. ACKNOWLEDGMENTS

The authors are indebted to D. F. Dücks and R. H. Dixon for providing supporting data on plasma conditions from a numerical model and from laser light scattering, respectively. Also, we are grateful to R. L. Kelly and C. P. Bhalla for providing, prior to publication, energies for excited states and transition probabilities, respectively, for both neon and oxygen ions. We also wish to thank J. R. McNally for permission to quote his similar experimental results prior to publication. Appreciation is expressed for the technical assistance of J. L. Ford in performing the plasma experiment and of E. Turbyfill in providing the automation necessary for long sequences of discharges and in assisting in the instrument calibration. Valuable discussions with H. R. Griem are recalled with appreciation.

*Some of the material in this paper has been used in a dissertation submitted in partial fulfillment of the requirements for the Doctor of Philosophy degree in the Astronomy Department at Georgetown University, 1971.

¹J. R. McNally, Oak Ridge National Laboratory (private communication).

²S. Glasstone and R. H. Lovberg, *Controlled Thermonuclear Reactions* (Van Nostrand, New York, 1960), Chap. 2, p. 31; also R. C. Elton, Naval Research Laboratory Report No. 6738, 1968 (unpublished).

³R. C. Elton, L. J. Palumbo, and H. R. Griem, *Phys. Rev. Lett.* **20**, 783 (1968).

⁴R. C. Elton and L. J. Palumbo, in *Proceedings of the International Conference on Inner-shell Ionization Phenomena*, 1972, U.S.AEC Report No. CONF-720404 (National Technical Information Service, Springfield, Va., 1973), p. 416; also Naval Research Laboratory Memorandum Report No. 2457, 1972 (unpublished); *Bull. Am. Phys. Soc.* **17**, 453 (1972); **17**, 1067 (1972).

⁵F. Bloch, *Phys. Rev.* **48**, 187 (1935).

⁶F. Bloch and P. A. Ross, *Phys. Rev.* **47**, 884 (1935).

⁷T. Åberg and J. Utriainen, *Phys. Rev. Lett.* **22**, 1346 (1969).

⁸J. W. Cooper and R. E. LaVilla, *Phys. Rev. Lett.* **25**, 1745 (1970).

⁹T. Åberg, *Phys. Rev. A* **4**, 1735 (1971).

¹⁰R. E. LaVilla, *Phys. Rev. A* **4**, 476 (1971).

¹¹T. Åberg, *Phys. Rev.* **156**, 35 (1967).

¹²J. S. Levinger, *Phys. Rev.* **90**, 11 (1953).

¹³A. Migdal, *J. Phys. (USSR)* **4**, 449 (1941); E. L. Feinberg, *J. Phys. (USSR)* **4**, 424 (1941); H. M. Schwartz, *J. Chem. Phys.* **21**, 45 (1953).

¹⁴M. O. Krause, *J. Phys. (Paris)* **32**, C4-67 (1971); M. O. Krause, T. A. Carlson, and W. E. Moddeman, *J. Phys. (Paris)* **32**, C4-139 (1971); T. A. Carlson, M. O. Krause, and W. E. Moddeman, *J. Phys.* **32**, C4-76 (1971); T. A. Carlson and M. O. Krause, *Phys. Rev.* **140**, A1057 (1965); M. O. Krause, T. A. Carlson, and R. D. Dismukes, *Phys. Rev.* **170**, 37 (1968).

¹⁵T. Åberg, in *Proceedings of the International Conference on Inner Shell Ionization Phenomena*, 1972, U.S.AEC Report No. CONF-720404 (National Technical Information Service, Springfield, Va., 1973), p. 1509; also Report No. 2/1972, Laboratory of Physics, Helsinki University of Technology (unpublished).

¹⁶Shake-up and shake-off are usually used to refer to the promotion of a bound electron through excitation to a higher bound level or through ionization, respectively, due to rearrangement following a sudden change in core potential. However, the two effects have at times been referred to collectively as shake-off, relative to electron removal from a particular orbital.

- ¹⁷T. A. Carlson, C. W. Nestor, Jr., T. C. Tucker, and F. B. Malik, *Phys. Rev.* **169**, 27 (1968).
- ¹⁸A. H. Gabriel and T. M. Paget, *J. Phys. B* **5**, 673 (1972).
- ¹⁹A. C. Kolb, W. H. Lupton, R. C. Elton, E. A. McLean, M. Swartz, M. P. Young, H. R. Griem, and E. Hintz, *Plasma Phys. Controlled Nucl. Fusion Res.* **1**, 261 (1966). The machine used in the present experiment is of lower energy (50 kJ) than that described in this reference and is of shorter length; however, the diameter and risetimes are similar.
- ²⁰L. J. Palumbo, Ph. D. dissertation (Georgetown University, 1971) (unpublished).
- ²¹R. H. Dixon, D. F. Dücks, and R. C. Elton, *Phys. Fluids* **16**, 1792 (1973).
- ²²Ruled and coated by Bausch and Lomb, Inc., Rochester N. Y.
- ²³M. A. Spivak, *Rev. Sci. Instr.* **41**, 1614 (1970).
- ²⁴M. A. Volkmar and R. L. Wolke, *Rev. Sci. Instr.* **40**, 849 (1969).
- ²⁵B. L. Henke, *X-Ray Optics and X-Ray Micro-Analysis*, edited by H. H. Pattee, V. E. Cosslett, and A. Engstrom (Academic, New York, 1963).
- ²⁶F. J. Morgan, A. H. Gabriel, and M. J. Barton, *J. Sci. Instr.* **1**, 998 (1968).
- ²⁷A. Bisi and L. Zappa, *Nuovo Cimento* **2**, 988 (1955); J. L. Campbell and K. W. D. Ledingham, *Brit. J. Appl. Phys.* **17**, 769 (1966); M. W. Charles and B. A. Cooke, *Nucl. Instr. Methods* **61**, 31 (1968).
- ²⁸W. Engelhardt, *Z. Phys.* **244**, 70 (1971).
- ²⁹M. Ehrlich and W. L. McLaughlin, *J. Opt. Soc. Am.* **46**, 797 (1956); L. S. Birks, R. R. Whitlock, J. S. Vierling, D. J. Nagel, and S. G. Gorbics, *J. Opt. Soc. Am.* **60**, 649 (1970).
- ³⁰N. V. Roth and R. C. Elton, Naval Research Laboratory Report No. 6638, 1968 (unpublished). The conditions under which the spectra in this report were obtained are very similar to those of the present study.
- ³¹R. L. Kelly with L. J. Palumbo, *Atomic and Ionic Emission Lines Below 2000 Å, Hydrogen through Krypton*, Naval Research Laboratory Report No. 7599 (U. S. GPO, Washington, D. C., 1973).
- ³²G. W. F. Drake, G. A. Victor, and A. Dalgarno, *Phys. Rev.* **180**, 25 (1969).
- ³³T. Åberg (private communication).
- ³⁴T. Åberg, *Ann. Acad. Sci. Fenn. A6* **308**, 1 (1969).
- ³⁵This somewhat simplified two-step model reduces enormously the complexity of the analysis by eliminating most multiple population channels, which would occur if the radiative decay and excitation were considered as a single dipole process including configuration interactions as allowed. The justification follows the analogy to the shake-up process, and the result is only a reduction in fine detail in the radiative-excitation-decay short-wavelength contribution, which would be blended by the folded-in instrumental broadening in any case.
- ³⁶S. M. R. Ansari, G. Elwert, and P. Mücklich, *Z. Naturforsch. A* **25**, 1781 (1970).
- ³⁷C. P. Bhalla, N. O. Folland, and M. A. Hein, *Phys. Rev. A* **8**, 649 (1973).
- ³⁸C. P. Bhalla (private communication).
- ³⁹A. H. Gabriel, *Mon. Not. R. Astron. Soc.* **160**, 99 (1972). Equation (7) of this reference is similar to Eq. (2) of this paper except for a numerical factor of 10^{-10} omitted in the former; also A. H. Gabriel and C. Jordan, *Nature* **221**, 947 (1969).
- ⁴⁰L. A. Vainshtein and U. I. Safronova, *Brief Communications in Physics: USSR*, No. 3, 40 (1972).
- ⁴¹C. W. Nestor, T. C. Tucker, T. A. Carlson, L. D. Roberts, F. B. Malik, and C. Froese, Oak Ridge National Laboratory Report No. ORNL-4027, 1966 (unpublished). (We are grateful to J. W. Cooper for bringing this report to our attention.)
- ⁴²U. I. Safronova and V. N. Kharitonova, *Opt. Spectrosc.* **27**, 300 (1969); also U. I. Safronova, A. N. Ivanova, N. V. Rabinkina, and V. N. Kharitonova, *Opt. Spectrosc.* **28**, 457 (1970). The energies calculated here are also in agreement with more limited calculations by F. P. Larkins [*J. Phys. B* **4**, 14 (1971)], and by Bhalla *et al.* (Ref. 37).
- ⁴³R. L. Kelly and D. E. Harrison, Jr., *Atom. Data* **3**, 177 (1971).
- ⁴⁴R. L. Kelly (private communication).
- ⁴⁵R. C. Elton, *Astrophys. J.* **148**, 573 (1967); G. W. F. Drake and A. Dalgarno, *Astrophys. J.* **157**, 459 (1969).
- ⁴⁶R. C. Elton, in *Plasma Physics*, Vol. 9, Pt. A of *Methods of Experimental Physics*, edited by H. R. Griem and R. H. Lovberg (Academic, New York, 1970).
- ⁴⁷H.-J. Kunze, *Space Sci. Rev.* **13**, 565 (1972).
- ⁴⁸R. C. Elton and W. W. Köppendörfer, *Phys. Rev.* **160**, 194 (1967).
- ⁴⁹H.-J. Kunze, A. H. Gabriel, and H. R. Griem, *Phys. Rev.* **165**, 267 (1968).
- ⁵⁰H.-J. Kunze and W. D. Johnston, III, *Phys. Rev. A* **3**, 1384 (1971).
- ⁵¹W. L. Wiese, M. W. Smith, and B. M. Glennon, *Atomic Transition Probabilities*, Report No. NSRDS-NBS-4 (U. S. GPO, Washington, D. C., 1966), Vol. 1.
- ⁵²Metastable initial-state population by rapid autoionization (where allowed) following dielectronic capture is not significant compared to direct excitation in the same species.
- ⁵³W. D. Johnston, III and H.-J. Kunze, *Phys. Rev. A* **4**, 962 (1971).
- ⁵⁴H. Van Regemorter, *Astrophys. J.* **136**, 906 (1962).
- ⁵⁵W. Engelhardt, W. Köppendörfer, and J. Sommer, *Phys. Rev. A* **6**, 1908 (1972).
- ⁵⁶A. Burgess, D. G. Hummer, and J. A. Tully, *Philos. Trans. R. Soc. Lond.* **266**, 225 (1970).
- ⁵⁷H.-J. Kunze, *Phys. Rev. A* **3**, 937 (1971).
- ⁵⁸N. F. Mott and H. S. W. Massey, *Theory of Atomic Collisions*, 3rd ed. (Clarendon, Oxford, 1965), Chap. 13, Pt. 4, and Chap. 15, Pt. 4.
- ⁵⁹J. R. Taylor, *Scattering Theory* (Wiley, New York, 1972), Chap. 13.
- ⁶⁰A. G. Sitenko, *Lectures in Scattering Theory* (Pergamon, New York, 1971), Chap. 7, pp. 107-113.
- ⁶¹A. H. Gabriel and C. Jordan, *Mon. Not. R. Astron. Soc.* **145**, 241 (1969).
- ⁶²See, e.g., D. Dücks and H. R. Griem, *Phys. Fluids* **9**, 1099 (1966). The authors are appreciative of Dr. Dücks for performing numerical calculations modeling this particular plasma. The results predict plasma conditions consistent with observations and also the evolution of the various ionic species present.
- ⁶³R. H. Dixon (private communication).
- ⁶⁴D. Dücks, W. Engelhardt, and W. Köppendörfer (to be published).